Indian Journal of Chemistry
Vol. 57A, March 2018, pp. 418-426

Arylazoimidazole complexes of lead(II)-halide and their photochromism

Debashis Mallick[a], Bharati Chowdhury[b], Chandana Sen[b], Kamal Krishna Sarkar[c], Srikanta Jana[b], Sudipa Mondal[b] & Chittaranjan Sinha[b,*]

[a]Department of Chemistry, Mrinalini Datta Mahavidyapith, Birati, Kolkata 700 051, India

[b]Department of Chemistry, Inorganic Chemistry Section, Jadavpur University, Kolkata 700 032, India

[c]Department of Chemistry, Mahadevananda Mahavidyalaya, SN Banerjee Rd, Monirampore, Kolkata, West Bengal 700120, India

Email: crsjuchem@gmail.com

Received 6 November 2017; revised and accepted 27 February 2018

Lead(II) complexes of 1-alkyl-2-(arylazo)imidazole (Raai-C_nH_{2n+1}), [Pb(Raai-C_nH_{2n+1})X_2] (X = Cl, Br, I; and Raai-C_nH_{2n+1}, R = H, Me and n = 4, 6, 8) have been characterized by UV-vis, IR and ^{1}H-NMR spectroscopy. The coordinated Raai-C_nH_{2n+1} in the complexes undergoes E-to-Z (*trans*-to-*cis*) isomerisation about the –N=N– group upon being irradiated with UV light in DMF solution. The rate and quantum yields of E-to-Z photoisomerisation ($\phi_{E\rightarrow Z}$) of the complexes are poorer than the respective free ligand response and are also affected by the nature of halide present (Cl^-, Br^- and I^-). Variation in physicochemical parameters may be correlated with the effective mass of the photochrome. The rate of isomerisation follows the sequence: [Pb(Raai-C_nH_{2n+1})Cl_2] < [Pb(Raai-C_nH_{2n+1})Br_2] < [Pb(Raai-C_nH_{2n+1})I_2]. The Z-to-E isomerisation has been carried out at varying temperatures (298–308 K) to determine the activation energy of Z-to-E (*cis*-to-*trans*) isomerisation (E_a: 47.09–63.42 kJ mol^{-1}) and the entropy of activation ($\Delta S^{\ddagger}$: 166.52 to –109.0 J mol^{-1} K^{-1}) which is a large negative in the complexes. Theoretical calculation supports cleavage of Pb(II)-N(azo) bond followed by the –N=N– rotation in a three-coordinated symmetry rather than the four-coordinated symmetry.

Keywords: Photochromism, Density functional calculations, Arylazoimidazoles, Lead halide complexes

In the study of the properties of hybrid functional materials[1], activation by irradiating light is of primary importance because of the reversible and non-destructive nature of the process. Light offers an attractive stimulus for external management of molecular switches and has vast advantages over other activation processes such as thermal, magnetic, mechanical, electrical and redox. Light driven structural changes between *trans* and *cis* isomers of azobenzene derivatives, defined as photochromism was reported by Hartley[2]. Since then, a large volume of work has been reported on the derivatives of azobenzene, the best characterized photoswitches[3-6]. Metal complexes of azo-conjugated ligand exhibit unique properties upon light irradiation in the area of photon-mode high-density information storage devices[7]. Arylazoimidazoles constitute a fascinating group of heterocyclic azo compounds because imidazole is a ubiquitous and essential group as a metal coordinating site[8-10]. Photochromism of arylazoimidazole[11-13] and their coordination complexes[14-20] has motivated us to examine the impact of light on hitherto unknown Pb(II) complexes of 1-alkyl-2-(arylazo)imidazoles (Raai-C_nH_{2n+1}, R = H, Me and n = 4 6, 8). The complexes have been spectroscopically characterized and optimized by DFT computation. The optical properties have been calculated by TDDFT computation.

Materials and Methods

$PbCl_2$, $PbBr_2$ and PbI_2 were obtained from Loba Chemicals, Bombay, India. 1-Alkyl-2-(arylazo) imidazoles were synthesized by reported procedure[21]. 1-Bromo-*n*-butane, 1-bromo-*n*-hexane and 1-bromo-*n*-octane, purchased from Sigma-Aldrich were of analytical reagent grade and were used as received. All other chemicals and solvents were of reagent grade and used as received. The solvents were purified before use by standard procedures[22].

Perkin-Elmer 2400 CHNS/O elemental analyzer was used to collect the C, H, N data. UV-vis spectra were recorded on a Perkin Elmer Lambda 25 spectrophoto meter and FTIR spectra (KBr disk, 4000-400 cm^{-1}) on a Perkin Elmer RX-1 FTIR spectrophotometer. Photoexcitation was carried out using a Perkin Elmer LS-55 spectrofluorometer while ^{1}H NMR spectra were

recorded on a Bruker (AC) 300 MHz FTNMR spectrometer.

Synthesis of complexes

Synthesis of [Pb(Haai-C_6H_{13})I_2] (11a)

PbI_2 (171 mg, 0.37 mmol) was added to ethyleneglycol monomethyl ether (EGME, 5 mL) followed by dropwise addition of 1-hexyl-2-(phenylazo)imidazole (100 mg, 0.37 mmol) to MeOH (15 mL) and refluxed for 2 h. The orange-red precipitate was collected by filtration, washed with KI solution (to remove excess of PbI_2) and then washed with MeOH and dried over $CaCl_2$ *in vacuo*. Crystallization was carried out by the slow evaporation of EGME-MeOH (1:4 *v/v*) solution to purify the products. The yield was 175 mg (66%). The other complexes were prepared under identical conditions and the yield varied in the range 63–72%.

$C_{13}H_{16}N_4Cl_2Pb$ (**4a**): Anal (%) Calc.: C, 30.82; H, 3.16; N, 11.06. Found: C, 30.85; H, 3.22; N, 11.14%. FT-IR (ν, cm^{-1}) 1589 (C=N), 1383 (N=N). UV-vis (λmax/nm, ε × 10^{-4} ($M^{-1}cm^{-1}$)) 369 (2.8), 377 (2.6), 453 (0.22).

$C_{14}H_{18}N_4Cl_2Pb$ (**4b**) : Anal (%) Calc.: C, 32.30; H, 3.46; N, 10.77. Found: C, 32.38; H, 3.40; N, 10.70%. FT-IR (ν, cm^{-1}) 1591 (C=N), 1385 (N=N). UV-vis (λmax/nm, ε × 10^{-4}($M^{-1}cm^{-1}$)) 367 (3.2), 381 (2.9), 452 (0.33).

$C_{15}H_{20}N_4Cl_2Pb$ (**5a**) : Anal (%) Calc.: C, 33.70; H, 3.74; N, 10.48. Found: C, 33.78; H, 3.70; N, 10.50%. FT-IR (ν, cm^{-1}) 1594 (C=N), 1379 (N=N). UV-vis (λmax/nm, ε × 10^{-4}($M^{-1}cm^{-1}$)) 366 (2.4), 383 (2.2), 461 (0.35).

$C_{16}H_{22}N_4Cl_2Pb$ (**5b**) : Anal (%) Calc.: C, 35.02; H, 4.01; N, 10.22. Found: C, 34.95; H, 4.00; N, 10.12%. FT-IR (ν, cm^{-1}) 1595 (C=N), 1440 (N=N). UV-vis (λmax/nm, ε × 10^{-4}($M^{-1}cm^{-1}$)) 368 (3.2), 381 (2.7), 459 (0.44).

$C_{17}H_{24}N_4Cl_2Pb$ (**6a**) : Anal (%) Calc.: C, 36.29; H, 4.27; N, 9.96. Found: C, 36.33; H, 4.20; N, 9.90%. FT-IR (ν, cm^{-1}) 1593 (C=N), 1379 (N=N). UV-vis (λmax/nm, ε × 10^{-4}($M^{-1}cm^{-1}$)) 367 (3.1), 382 (2.9), 451 (0.30).

$C_{18}H_{26}N_4Cl_2Pb$ (**6b**) : Anal (%) Calc.: C, 37.49; H, 4.51; N, 9.72. Found: C, 37.43; H, 4.45; N, 9.98%. FT-IR (ν, cm^{-1}) 1594 (C=N), 1382 (N=N). UV-vis (λmax/nm, ε × 10^{-4}($M^{-1}cm^{-1}$)) 366 (2.7), 377 (2.3), 460 (0.24).

$C_{13}H_{16}N_4Br_2Pb$ (**7a**) : Anal (%) Calc.: C, 26.22; H, 2.69; N, 9.41. Found: C, 26.27; H, 2.73; N, 9.47%. FT-IR (ν, cm^{-1}) 1594 (C=N), 1382 (N=N). UV-vis (λmax/nm, ε × 10^{-4}($M^{-1}cm^{-1}$)) 366 (2.7), 377 (2.3), 460 (0.24).

$C_{14}H_{18}N_4Br_2Pb$ (**7b**) : Anal (%) Calc.: C, 27.59; H, 2.96; N, 9.20. Found: C, 27.63; H, 3.04; N, 9.24%. FT-IR (ν, cm^{-1}) 1595 (C=N), 1383 (N=N). UV-vis (λmax/nm, ε ×10^{-4}($M^{-1}cm^{-1}$)) 367 (2.6), 380 (2.2), 462 (0.35).

$C_{15}H_{20}N_4Br_2Pb$ (**8a**) : Anal (%) Calc.: C, 28.89; H, 3.21; N, 8.99. Found: C, 28.91; H, 3.27; N, 8.95% . FT-IR (ν, cm^{-1}) 1590 (C=N), 1379 (N=N). UV-vis (λmax/nm, ε × 10^{-4}($M^{-1}cm^{-1}$)) 365 (3.1), 379 (2.5), 462 (0.26).

$C_{16}H_{22}N_4Br_2Pb$ (**8b**) : Anal (%) Calc.: C, 30.14; H, 3.45; N, 8.79. Found: C, 29.98; H, 3.48; N, 8.82%. FT-IR (ν, cm^{-1}) 1597 (C=N), 1383 (N=N). UV-vis (λmax/nm, ε × 10^{-4}($M^{-1}cm^{-1}$)) 366 (2.8), 383 (2.4), 455 (0.24).

$C_{17}H_{24}N_4Br_2Pb$ (**9a**) : Anal (%) Calc.: C, 31.34; H, 3.66; N, 8.60 Found: C, 31.30; H, 3.73; N, 8.63% . FT-IR (ν, cm^{-1}) 1598 (C=N), 1378 (N=N). UV-vis (λmax/nm, ε × 10^{-4}($M^{-1}cm^{-1}$)) 369 (2.6), 375 (2.1), 459 (0.25).

$C_{18}H_{26}N_4Br_2Pb$ (**9b**) : Anal (%) Calc.: C, 32.48; H, 3.91; N, 8.42. Found: C, 32.53; H, 384; N, 8.45%. FT-IR (ν, cm^{-1}) 1596 (C=N), 1383 (N=N). UV-vis (λmax/nm, ε × 10^{-4}($M^{-1}cm^{-1}$)) 367 (2.5), 380 (2.0), 453 (0.30).

$C_{13}H_{16}N_4I_2Pb$ (**10a**) : Anal (%) Calc.: C, 22.63; H, 2.32; N, 8.13. Found: C, 22.66; H, 2.27; N, 8.19%. FT-IR (ν, cm^{-1}) 1580 (C=N), 1380 (N=N). UV-vis (λmax/nm, ε × 10^{-4}($M^{-1}cm^{-1}$)) 366 (2.5), 381 (2.13), 451 (0.36).

$C_{14}H_{18}N_4I_2Pb$ (**10b**) : Anal (%) Calc.: C, 23.89; H, 2.56; N, 7.96. Found: C, 23.85; H, 2.53; N, 7.89%. FT-IR (ν, cm^{-1}) 1582 (C=N), 1381 (N=N). UV-vis (λmax/nm, ε × 10^{-4}($M^{-1}cm^{-1}$)) 368 (1.91), 383 (1.68), 450 (0.22).

$C_{15}H_{20}N_4I_2Pb$ (**11a**) : Anal (%) Calc.: C, 25.10; H, 2.79; N, 7.80. Found: C, 25.13; H, 2.83; N, 7.70%. FT-IR (ν, cm^{-1}) 1587 (C=N), 1378 (N=N). UV-vis (λmax/nm, ε × 10^{-4}($M^{-1}cm^{-1}$)) 368 (1.89), 382 (1.85), 449 (0.27).

$C_{16}H_{22}N_4I_2Pb$ (**11b**) : Anal (%) Calc.: C, 26.26; H, 3.01; N, 7.66 Found: C, 26.20; H, 3.06; N, 7.60%. FT-IR (ν, cm^{-1}) 1590 (C=N), 1379 (N=N). UV-vis (λmax/nm, ε × 10^{-4}($M^{-1}cm^{-1}$)) 366 (1.85), 381 (1.75), 452 (0.35).

$C_{17}H_{24}N_4I_2Pb$ (**12a**) : Anal (%) Calc.: C, 27.38; H, 3.22; N, 7.51. Found: C, 27.44; H, 3.27; N, 7.58%. FT-IR (ν, cm^{-1}) 1587 (C=N), 1378 (N=N). UV-vis

(λmax/nm, ε × 10^{-4}($M^{-1}cm^{-1}$)) 368 (1.89), 382 (1.88), 450 (0.27).

$C_{18}H_{26}N_4I_2Pb$ (**12b**) : Anal (%) Calc.: C, 28.45; H, 3.42; N, 7.38. Found: C, 28.50; H, 3.39; N, 7.30%. FT-IR (ν, cm^{-1}) 1585 (C=N), 1380 (N=N). UV-vis (λmax/nm, ε × 10^{-4}($M^{-1}cm^{-1}$)) 367 (1.83), 383 (1.79), 451 (0.35).

Photometric measurements

A 1×1 cm quartz optical cell maintained at 25 °C with a Peltier thermostat in Perkin Elmer Lambda 25 UV/vis spectrophotometer was used for absorption spectral measurements. Perkin Elmer LS 55 spectrofluorometer, with a Xenon lamp (slit width 10 nm) as a source of light (150 W) for excitation was used. An optical filter was used to cut off overtones when necessary. Quantum yields (ϕ) were calculated by measuring E-to-Z (*trans*-to-*cis*) isomerization rates (ν) in a well-stirred solution using the relation, $\nu = (\phi I_0/V)(1–10^{-Abs})$ where I_0 is the photon flux at the front of the cell, V is the volume of the solution, and Abs is the initial absorbance at the irradiation wavelength. The value of I_0 was obtained by using azobenzene (ϕ = 0.11 for π-π* excitation[23]) under the same conditions of irradiation.

The Z-to-E (*cis*-to-*trans*) isomerisation rates were obtained by monitoring the absorption changes intermittently for a Z-rich solution kept in the dark at constant temperatures (T) in the range of 298-308 K. The activation energy (E_a) was obtained from $\ln k = \ln A – E_a/RT$, where k is rate constant, R is gas constant, and T is temperature. The values of activation enthalpy ($\Delta H^{\ddagger}$) and activation entropy ($\Delta S^{\ddagger}$) were obtained from the Eyring plot using Eq. 1 and $\Delta G^{\ddagger} = E_a – RT – T\Delta S^{\ddagger}$ where k_B and h are Boltzmann's and Plank's constants respectively.

$$\ln \frac{k}{T} = \frac{-\Delta H^{\ddagger}}{R} \cdot \frac{1}{T} + \ln \frac{k_B}{h} + \frac{\Delta S^{\ddagger}}{R}$$

Computational procedure

The structures of [Pb(MeaaiC$_6$H$_{13}$)X$_2$] (X = Cl (**5b**), Br (**8b**), I (**11b**)) were optimized by DFT computation using GAUSSIAN 03 (G03) program package[24] and following the B3LYP exchange correlation functional[25] and Los Alamos effective core potential plus double zeta (LanL2DZ)[26-28] basis set along with the corresponding pseudo potential without any symmetry constrain for lead, bromide and iodide. The vibrational frequency calculation was performed to ensure the optimized geometries with the local minima; only positive Eigen values were considered. The TDDFT[29] calculations were performed to assign the low lying electronic transitions in the experimental spectra. The results of lowest 25 singlet–singlet transitions and those of TDDFT calculations were qualitatively very similar. The fractional contributions of various groups to each molecular orbital were calculated by GaussSum[30].

Results and Discussion

Synthesis and formulation of the compounds

[Pb(Raai-C_nH_{2n+1})X_2] (**4-12**) (Scheme 1; Raai-C_nH_{2n+1}, **1-3**, where R = H (**a**), Me (**b**); n = 4 (C_4H_9, **1**), 6 (C_6H_{13}, **2**), 8 (C_8H_{17}, **3**)) and X = Cl, Br, I)) were characterized by microanalytical (C, H, N) and vibrational spectroscopic data[19,20]. We could not isolate X-ray diffraction quality single crystal of the present series of complexes for accurate structure determination. The N(1)–alkylation is approved by the disappearance of δ(N–H) (10.30 ppm) of imidazolyl-N(1)H and the appearance of N(1)-alkyl signal at 0.85–4.40 ppm. The triplet signal of –CH_2– at 4.40 ppm, multiplet for –$(CH_2)_n$– at 1.22-1.90 ppm and a triplet at 0.85 ppm (–CH_3 group) refer to the –N–CH_2–$(CH_2)_n$–CH_3 group. Imidazolyl 4-H appears at 7.24-7.28 ppm and 5-H appears at 7.14–7.17 ppm which are broadened perhaps due to the rapid exchange with solvent. Aryl-Hs are affected by –Me substitution;

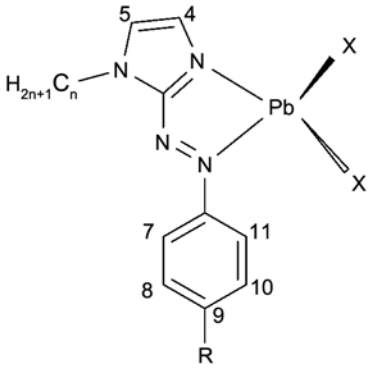

[Pb(Raai-C_nH_{2n+1})X_2] (**4-12**)

Raai-C_nH_{2n+1} (**1-3**); R = H (**a**), Me (**b**) and n = 4 (**1**), 6 (**2**), 8 (**3**)

R = H, n = 4, X = Cl (**4a**); R = Me, n = 4, X = Cl (**4b**);
R = H, n = 6, X = Cl (**5a**); R = Me, n = 6, X = Cl (**5b**);
R = H, n = 8, X = Cl (**6a**); R = Me, n = 8, X = Cl (**6b**);
R = H, n = 4, X = Br (**7a**); R = Me, n = 4, X = Br (**7b**);
R = H, n = 6, X = Br (**8a**); R = Me, n = 6, X = Br (**8b**);
R = H, n = 8, X = Br (**9a**); R = Me, n = 8, X = Br (**9b**);
R = H, n = 4, X = I (**10a**); R = Me, n = 4, X = I (**10b**);
R = H, n = 6, X = I (**11a**); R = Me, n = 6, X = I (**11b**);
R = H, n = 8, X = I (**12a**); R = Me, n = 8, X = I (**12b**)

Scheme 1

the aryl protons (7-H to 11-H) move upfield on going from phenylazo (a) to *p*-tolylazo (b) (Table S1 and Supplementary Data, Figs S1-S3). Imidazolyl-Hs (4-, 5-H) of coordinated Raai-C_nH_{2n+1} to Pb(II) shift downfield by 0.3-0.4 ppm compared to the free ligand position. This supports the strong preference of binding of imidazolyl-N to Pb(II). Mass peak (HRMS spectrum) of one of the complexes, $[Pb(Meaai\text{-}C_6H_{13})I_2]_n$ (Supplementary Data, Fig. S4) supports the calculated data. [(*m/z*, 732.48 (experimental); 731.97 (calc.)].

Spectral studies and photochromism

The intense absorption band at 340–380 nm (ε, 10^3 dm^3 mol^{-1} cm^{-1}) of Raai-C_nH_{2n+1} (DMF solution) is assigned to the π-π* transition and weak band at 450-455 nm[31] to the n-π* transition. In the complexes, the bands at 364-368 nm and 460-465 nm refer to π-π* and n-π* transitions. Upon UV light irradiation (λ, 364–368 nm) of the complexes in DMF solution, the E-to-Z (*trans*-to-*cis*) isomerisation of coordinated Raai-C_nH_{2n+1} is observed as shown in Fig. 1. The *trans*-to-*cis* photoisomerisation takes place and the *cis* molar ratio reaches up to >95%. Photoisomerisation of representative ligand is shown in Fig. S5, Supplementary Data; see also Table S2 and S3. The wavelength required for irradiation for the free ligand does not show any significant shift (1–3 nm) which undoubtedly indicates little electronic influence of coordinated metal ion. However, other photophysical data like rate of isomerisation, quantum yields, activation energy barrier etc., i.e., the properties that depend on mass of the molecule are affected prominently. On repeated irradiation, even after 15 cycles, the photochrome does not show any change of intensity which suggests photostability of the analyte (Supplementary Data, Fig. S6). The quantum yields of *trans*-to-*cis* ($\phi_{E\to Z}$) photoisomerisation of complexes are recorded in Table 1. The rate and quantum yields of E-to-Z isomerisation of the complexes are less than that of free ligand data. The $\phi_{E\to Z}$ values are significantly dependent on the nature of the substituents and halide substituents. The Me substituent at Ar-N=N– and also substituent at N(1)-position (1-C_nH_{2n+1}) decreases the $\phi_{E\to Z}$ values. In general, increase in the rotor-mass of the complexes diminishes the rate of E-to-Z isomerisation. The lowering of $\phi_{E\to Z}$ in the complexes may be due to the presence of coordinated PbX_2 that increases molecular weight and severely interferes with the motion of the –N=N-Ar moiety. Also, the photo bleaching efficiency

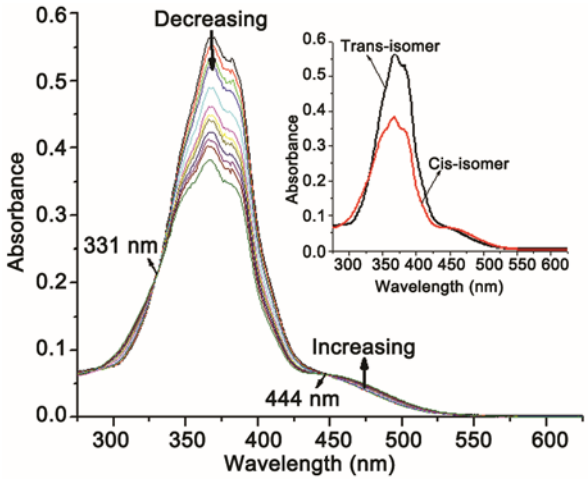

Fig. 1 — The spectral changes of $[Pb(Meaai\text{-}C_6H_{13})I_2]$ (**11b**) in DMF solution upon repeated irradiation at 368 nm at 5 min interval at 25 °C. [Inset shows spectra of *cis* and *trans* isomer of the complex.]

of halide may deplete the energy of the π-π* excited state. These may also cause very fast deactivation in addition to the photochromic route. Both rotor mass and volume are increased upon coordination of ligand to PbX_2. These two factors have a significant influence on the isomerisation rate and quantum yields.

The Z-to-E (*cis*-to-*trans*) isomerisation of the complexes was observed in the temperature range of 298-308 K. A subtle change in spectral pattern is observed with change in temperature as shown in Fig. 2. From the linear Eyring plots in the range of 298-308 K (Supplementary Data, Fig. S7) the activation energies were calculated and are recorded in Table 2. In the complexes, the E_as are substantially decreased, which means faster Z-to-E isomerisation of the complexes. The entropy of activation ($\Delta S^{\ddagger}$) essentially shows higher negative value in the complexes as compared to that in the free ligand. This thermodynamic data indeed show that increase in the effective mass of rotor decreases the photoisomerisation probability.

Electronic structure and optical spectra

The optimized structures of $[Pb(Meaai\text{-}C_6H_{13})X_2]$ (X = Cl (**5b**), Br (**8b**), I (**11b**)) were used for DFT computation and analyses of molecular functions. The occupied MOs (HOMO, HOMO-1, etc.) in the complexes are dominated by X (HOMO shares 74% Cl (**5b**), 84% Br (**8b**), 94% I (**11b**)) and HOMO-1, HOMO-2, etc. contain >90% of the halide (Fig. 3). The LUMO, LUMO+1, LUMO+2 have received the major share from coordinated Meaai-C_6H_{13} (>95%)

Table 1 — Photochromism, rate of conversion and quantum yields upon UV light irradiation

Comp.	λ_{π,π^*} (nm)	Isobestic point (nm)	Rate of E→Z conv.×10^8 (s^{-1})	$\phi_{E\rightarrow Z}$ conv.
4a	365	335,437	1.53	0.083
4b	366	336,446	1.42	0.079
5a	365	334,443	1.33	0.074
5b	364	337,444	1.30	0.073
6a	367	333,442	1.23	0.069
6b	365	336,441	1.21	0.068
7a	366	333,435	1.67	0.091
7b	366	331,447	1.54	0.089
8a	368	334,441	1.53	0.085
8b	367	333,440	1.51	0.084
9a	369	336,433	1.48	0.081
9b	366	331,442	1.31	0.077
10a	368	337,443	1.87	0.099
10b	368	338,445	1.80	0.097
11a	364	335,433	1.76	0.095
11b	365	331,444	1.67	0.092
12a	365	335,441	1.59	0.090
12b	367	337,444	1.54	0.089

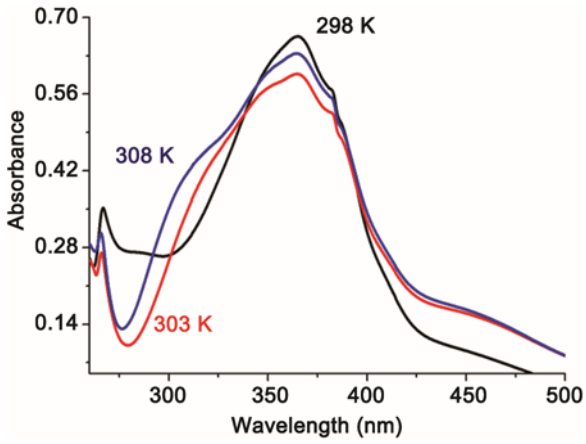

Fig. 2 — The Z-E transformation UV spectra at different temperatures (298, 303, 308 K) of $[Pb(Meaai\text{-}C_6H_{13})I_2]_n$ (**11b**)

(Supplementary Data, Fig. S8 and Tables S3, S5 and S7). The azo group shares 45–52% in the unoccupied MOs of Meaai-C_6H_{13}.

The spectral transitions were theoretically calculated and show that longer wavelength transitions (>450 nm) refer to X (Cl, Br or I) → π*(azoimine) charge transfer transitions (Supplementary Data, Tables S4, S6 and S8). The calculated MLCT transition appears at < 412 nm. A strong π–π* transition (HOMO-8/ HOMO-7 to LUMO+1) is expected around 325–375 nm. UV light irradiation is only responsible for isomerisation from the more stable *trans*-isomer (E) to the less stable *cis*-isomer (Z). The UV light absorption by the complex may be responsible for the π-π* transition to coordinated Raai-C_nH_{2n+1} followed by cleavage of Pb(II)-N(azo) bond. The structure determination of Pb(II)-azoimidazole complex[32] supports the longer Pb-N(azo) distance (2.743 Å) as compared to Pb-N(imidazolyl) (2.414 Å) although both the nitrogens are N(sp^2). This supports the weakening of the Pb-N(azo) distance. Theoretical (DFT) calculations also support this conjecture. The MLCT or XLCTs are of lower energetic transitions and capable of assisting charge transfer to azoimidazole but may not be sufficient for Pb-N(azo) dissociation or rotation about –N=N– bond leading to isomerisation. Conversely, charge transition in the excited complex may take place in a secondary (MLCT or XLCT) process, which is responsible for the deactivation of excited species and reduction in the rate of *trans* → *cis* change and quantum yields as shown in Table 1. Theoretical calculations show that the four-coordinated Pb(II) complex is unstable (Hartree energy (Ha) = –860.2560934 = –23408.7693323 eV) by 215 eV as compared to the three-coordinated Pb(II) complex (Ha = –868.1753541 = –23624.25814 eV) intermediate (Supplementary Data, Fig. S9 and Tables S9, S10). Hence, cleavage followed by rotation (Scheme 2) may be the probable mechanism of photoisomerisation herein.

The correlation diagram (Fig. 4) shows that the energy difference between HOMO and LUMO decreases with declining electronegativity of Cl to Br

Table 2 — Rate and activation parameters for Z (*cis*) → E (*trans*) thermal isomerisation

Comp.	Temp. (K)	Rate of thermal Z→E conv.×10^3 (s^{-1})	E_a (kJ mol^{-1})	$\Delta H^{\ddagger}$ (kJ mol^{-1})	$\Delta S^{\ddagger}$ (J $mol^{-1}K^{-1}$)	$\Delta G^{\ddagger}$ (kJ mol^{-1})
4a	298	0.1531	51.54	49.03	-153.48	95.92
	303	0.2115				
	308	0.3009				
4b	298	0.1588	51.05	48.54	-154.82	95.44
	303	0.2190				
	308	0.3101				
5a	298	0.1699	50.46	47.94	-156.38	95.33
	303	0.2216				
	308	0.3294				
5b	298	0.1768	50.20	47.68	-156.63	95.14
	303	0.2563				
	308	0.3412				
6a	298	0.1804	48.87	46.36	-160.89	95.10
	303	0.2624				
	308	0.3421				
6b	298	0.1864	47.09	44.57	-166.52	95.03
	303	0.2756				
	308	0.3452				
7a	298	0.2008	55.52	53.00	-137.69	94.73
	303	0.3031				
	308	0.4155				
7b	298	0.2013	55.07	52.55	-139.11	94.70
	303	0.3135				
	308	0.4139				
8a	298	0.2076	54.48	51.96	-140.75	94.60
	303	0.3325				
	308	0.4234				
8b	298	0.2086	54.28	51.73	-141.57	94.62
	303	0.3235				
	308	0.4243				
9a	298	0.2213	53.03	50.51	-145.67	94.65
	303	0.2835				
	308	0.4439				
9b	298	0.2221	52.85	50.33	-146.24	94.64
	303	0.2829				
	308	0.4445				
10a	298	0.2563	63.42	60.91	-109	94.15
	303	0.4129				
	308	0.5881				
10b	298	0.2464	63.04	60.53	-110.16	94.04
	303	0.4135				
	308	0.5623				
11a	298	0.2342	62.94	60.44	-111.50	94.41
	303	0.3591				
	308	0.5342				
11b	298	0.2346	62.88	60.37	-111.78	94.24
	303	0.3605				
	308	0.5348				
12a	298	0.2566	62.52	60.01	-112.24	94.02
	303	0.3933				
	308	0.5822				
12b	298	0.2376	61.66	59.15	-115.45	94.13
	303	0.3415				
	308	0.5334				

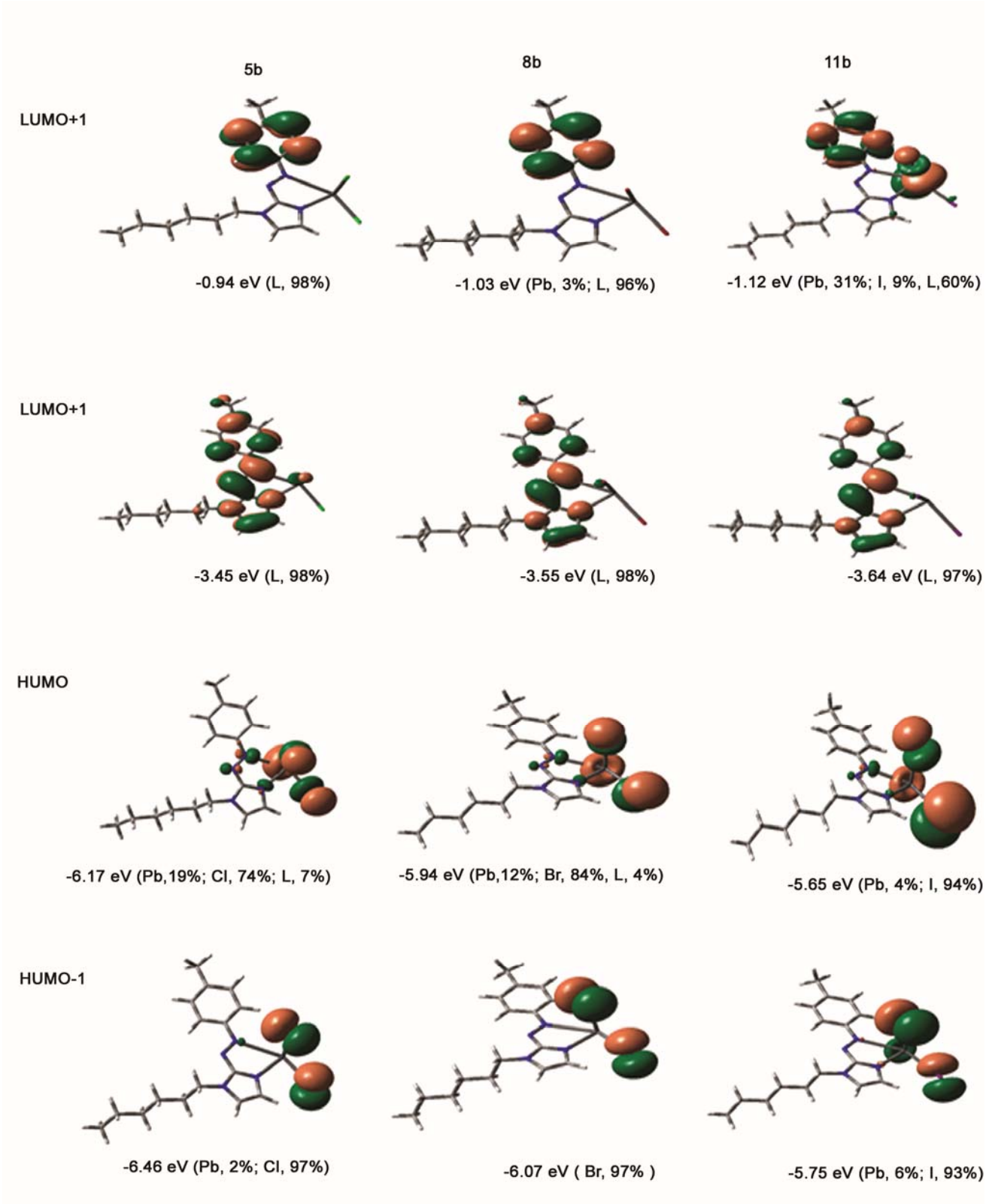

Fig. 3 — Surface plots of HOMO, HOMO-1, LUMO and LUMO+1 of [Pb(Meaai-C_6H_{13})Cl_2] (**5b**), [Pb(Meaai-C_6H_{13})Br_2] (**8b**), and [Pb(Meaai-C_6H_{13})I_2] (**11b**).

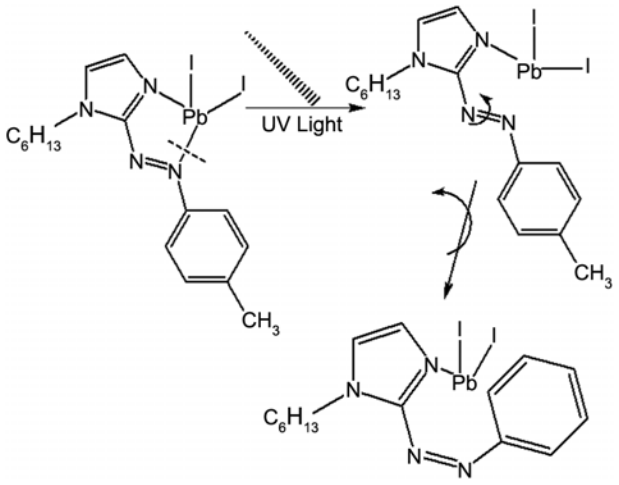

Scheme 2

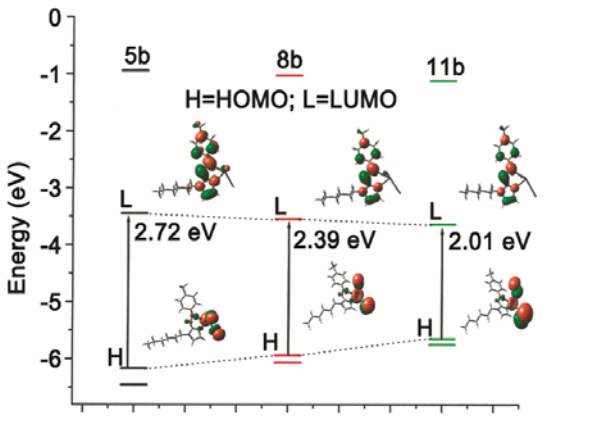

Fig. 4 — Energy correlation between HOMO (H), HOMO-1 (H-1), LUMO (L) and LUMO+1 (L+1) of [Pb(Meaai-C_6H_{13})Cl_2] (**5b**); [Pb(Meaai-C_6H_{13})Br_2] (**8b**); [Pb(Meaai-C_6H_{13})I_2] (**11b**). [Results obtained from DFT calculation of optimized geometries].

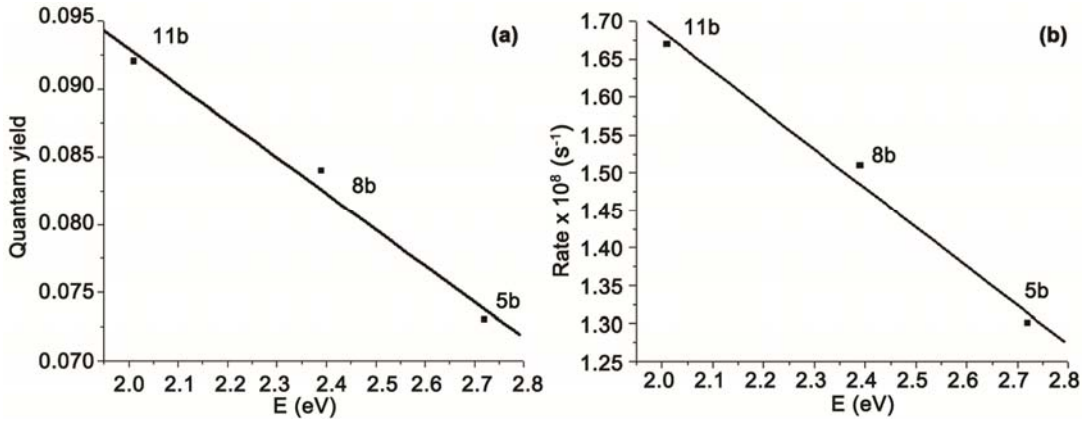

Fig. 5 — Correlation between E (= E_{LUMO}–E_{HOMO}) and quantum yields (*trans*-to-*cis*), and (b) E and rate of thermal process (*cis*-to-*trans*).

to I: {[Pb(Meaai-C_6H_{13})Cl_2] (2.72 eV), [Pb(Meaai-C_6H_{13})Br_2] (2.39 eV) and [Pb(Meaai-C_6H_{13})I_2] (2.01 eV)}. The plots of ΔE versus rates of isomerisation and quantum yields are linearly related (Fig. 5), indicating the direct correlation between the photophysical process and activation energy barrier.

Conclusions

The solution of [Pb(Raai-C_nH_{2n+1})X_2] (1-alkyl-2-(arylazo)imidazoles, Raai-C_nH_{2n+1} where n = 4, 6 and 8; X = Cl, Br, I) in DMF were optically stimulated and photoisomerisation of coordinated Raai-C_nH_{2n+1} was observed via –N=N– bond. The rate and quantum yields of photo-isomerisation of the complexes were determined. The activation energy (E_a) of isomerisation of the free ligand is three times that of the complexes, indicating that the lowering of rate in the complexes may be due to higher molar mass of the complexes as compared to that of the free ligand.

Supplementary Data

Supplementary Data associated with this article are available in the electronic form at http://www.niscair.res.in/jinfo/ijca/IJCA_57A(03)418-426_SupplData.pdf.

Acknowledgement

Financial support under minor research programme (PSW-158/13-14) from the UGC, New Delhi, India and the Council of Scientific and Industrial Research (CSIR, Sanction No. 01(2894)/17/EMR-II) New Delhi, India, are gratefully acknowledged.

References

1 *Functional Hybrid Materials*, edited by P Gómez-Romero & C Sanchez, (Wiley-VCH Verlag GmbH, Weinham, Germany) 2004.

2 *New Frontiers in Photochromism*, edited by N Tamaoki, M Irie, Y Yokoyama & T Seki, (Springer, Japan) 2013.

3 *Photochromism Molecules and Systems*, edited by H Durr & H Bouas-Laurent, (Elsevier, Amsterdam) 2003.
4 Knoll H, CRC Handbook of *Organic Photochemistry and Photobiology*, edited by W Horspool & F Lenci, (CRC Press, Boca Raton) 2004, p. 1.
5 *Photochromism: Memories and Switches (Special Issue), Chem Rev*, 100 (2000)1683.
6 Wang R, Zhang X, Pua S, Liu G & Dai Y, *Spectrochim Acta A*, 173 (2017) 257.
7 Ire M, *Chem* Rev,100 (2000) 1683.
8 Ray U, Banerjee D, Mostafa G, Lu T–H & Sinha C, *New J Chem*, 28 (2004) 1437.
9 Dinda J, Jasimuddin S, Mostafa G, Hung C H & Sinha C, *Polyhedron*, 23 (2004) 793.
10 Chand B, Ray U, Mostafa G, Cheng J, Lu T H & Sinha C, *Inorg Chim Acta*, 358 (2005) 1927.
11 Otsuki J, Suwa K, Narutaki K, Sinha C, Yoshikawa I & Araki K, *J Phys Chem A*,109 (2005) 8064.
12 Gayen P & Sinha C, *J Indian Chem Soc*, 90 (2013) 751.
13 Gayen P & Sinha C, *Spectrochim Acta A*, 104 (2013) 477.
14 Sen C, Nandi A, Mallick D, Mondal S, Sarker K K & Sinha C, *Spectrochim Acta A*, 137 (2015) 935.
15 Sen C, Mallick D, Mondal S & Sinha C, *J Indian Chem Soc*, 92 (2015) 203.
16 Nandi A, Sen C, Roy S, Mallick D, Sinha R, Mondal T K & Sinha C, *Polyhedron*, 79 (2014) 186.
17 Misra T K, Das D, Sinha C, Ghosh P K & Pal C K, *Inorg Chem*, 37 (1998) 1672 .
18 Mondal J A, Saha G, Sinha C & Palit D K, *Phys Chem Chem Phys*, 14 (2012) 13027.
19 Mallick D, Sarker K K, Datta P, Mondal T K & Sinha C, *Inorg Chim Acta*, 387 (2012) 352.
20 Sarker K K, Jana A D , Mostafa G, Wu J-S, Lu T-H, & Sinha C, *Inorg Chim Acta,* 359 **(**2006**)** 4377.
21 Saha (Halder) S, Roy S, Mondal T K, Saha R, & Sinha C, *Z Anorg Alleg Chem*, 639 (2013) 1861.
22 Vogel A I, *A Text-Book* of *Quantitative Inorganic Analysis*, 3rd Edn, (ELBS, Longman) 1975, p. 433.
23 Zimmerman G, Chow L & Paik U, *J Am Chem Soc*, 80 (1958) 3528.
24 *Gaussian 03, Revision C 02*, (Gaussian, Inc, Wallingford CT) 2004.
25 B3LYP, Becke A D , *J Chem Phys*, 98 (1993) 5648.
26 LanL2DZ, Hay P J & Wadt W R, *J Chem Phys*, 82 (1985) 299.
27 Wadt W R & Hay P J , *J Chem Phys*, 82 (1985) 284.
28 Hay P J & Wadt W R, *J Chem Phy*, 82 (1985) 270.
29 *EMSL*, Basis set library from http:/www.emsl.pnl.gov/forms/basisform.html.
30 Boyle N M O & Vos J G, *GaussSum* 1.0, (Dublin City University, Dublin, Ireland) 2005. Available from http://gausssum.sourceforge.net.
31 Mallick D, Nandi A, Datta S, Sarker K K, Mondal T K & Sinha C, *Polyhedron*, 31 (2012) 506.
32 Mallick D, Nandi A, Sarker K K, Datta P, Mondal T K, & Sinha C, *Inorg Chim Acta*, 387 (2012) 352.